REPORT DOCUMENTATION PAGE

Form Approved
OMB No. 0704-0188

1. REPORT DATE *(DD-MM-YYYY)*	**2. REPORT TYPE**	**3. DATES COVERED** *(From - To)*
17-04-2008	FINAL	04/15/04 – 12/31/07

4. TITLE AND SUBTITLE
Self Assembled Semiconductor Quantum Dots for Spin Based all Optical and Electronic Quantum Computing

5a. CONTRACT NUMBER
N/A

5b. GRANT NUMBER
FA9550-04-1-0261

5c. PROGRAM ELEMENT NUMBER

6. AUTHOR(S)
Bandyopadhyay, Supriyo; Morkoc, Hadis

5d. PROJECT NUMBER

5e. TASK NUMBER

5f. WORK UNIT NUMBER

7. PERFORMING ORGANIZATION NAME(S) AND ADDRESS(ES)

Virginia Commonwealth Univ
School of Engineering
PO Box 843068
Richmond, VA 23284-3068

8. PERFORMING ORGANIZATION REPORT NUMBER

529205; PT090241

9. SPONSORING / MONITORING AGENCY NAME(S) AND ADDRESS(ES)
AFOSR
Attn: Wendy Veon - PKC
875 N Randolph St
Suite 325, Rm 3112
Arlington, VA 22203-1768

10. SPONSOR/MONITOR'S ACRONYM(S)

11. SPONSOR/MONITOR'S REPORT NUMBER(S)

12. DISTRIBUTION / AVAILABILITY STATEMENT

APPROVED FOR PUBLIC RELEASE

13. SUPPLEMENTARY NOTES

14. ABSTRACT

This project involved the study of self assembled quantum dots as hosts for spin-based qubits. Both semiconductor quantum dots, nanowires, and organic quantum dots were studied and the spin relaxation times were measured. The organic Alq_3 appears to have very long longitudinal spin relaxation time of nearly 1 second at a temperature of 100 K, and a nearly temperature independent transverse relaxation time > 3 nsec in the range 2 – 300 K. This relaxation time is sufficient to fulfill the Knill criterion for fault-tolerant quantum computing at room temperature. Since organics have special selection rules for radiative transitions whereby triplet electron-hole pairs are dark excitons and only singlets are radiative, there is a natural qubit read out scheme for organic quantum dots. We have also studied inorganic semiconductor quantum dots, but find them inferior to their organic counterparts for spin based quantum computing, primarily because spin-orbit interactions are much stronger in inorganic quantum dots, leading to much faster spin dephasing.

15. SUBJECT TERMS
Spintronics, quantum dots, self assembly

16. SECURITY CLASSIFICATION OF:			**17. LIMITATION OF ABSTRACT**	**18. NUMBER OF PAGES**	**19a. NAME OF RESPONSIBLE PERSON**
a. REPORT	**b. ABSTRACT**	**c. THIS PAGE**			Supriyo Bandyopadhyay
Unclassified	Unclassified	Unclassified	SAR		**19b. TELEPHONE NUMBER** *(include area code)* (804) 827-6275

Self Assembled Semiconductor Quantum Dots for Spin Based All Optical and Electronic Quantum Computing

Grant No: FA9550-04-1-0261

PI: Supriyo Bandyopadhyay
Department of Electrical Engineering
Virginia Commonwealth University
601 W. Main Street
Richmond, VA 23284, USA
Tel: (804) 827-6275
E-mail: sbandy@vcu.edu

Co-PIs
Alison Baski and Shiv Khanna
Department of Physics
Hadis Morkoc
Department of Electrical and Computer Engineering
Virginia Commonwealth University
601 W. Main Street
Richmond, VA 23284

Objectives: The original objective of this program is to fabricate, characterize and study self assembled semiconductor quantum dots and wires for *spin-based* all optical and electronic quantum computing.

Result of effort: The main advances are listed below:

Organics as qubit hosts:

The important figure of merit for quantum dots acting as hosts for spin based qubits is the spin relaxation time – both longitudinal and transverse relaxation times T_1 and T_2.

T_1 time: During the tenure of this project, we showed that the π-conjugated organic tris (8-hydroxy-quinolinolato aluminum) also known as Alq_3, has an exceptionally long spin relaxation time T_1 exceeding 1 second at a temperature of 100 K [1]. This is the longest T_1 time reported in any nanostructured system to date. Fig 1 shows a cross-section TEM of a nanowire spin valve structure with an organic quantum dot in the middle that was used to measure this time and Fig. 2 shows the measured spin diffusion length and longitudinal spin relaxation time (T_1) as a function of temperature. This result establishes organic semiconductors as excellent platforms for spin based computing.

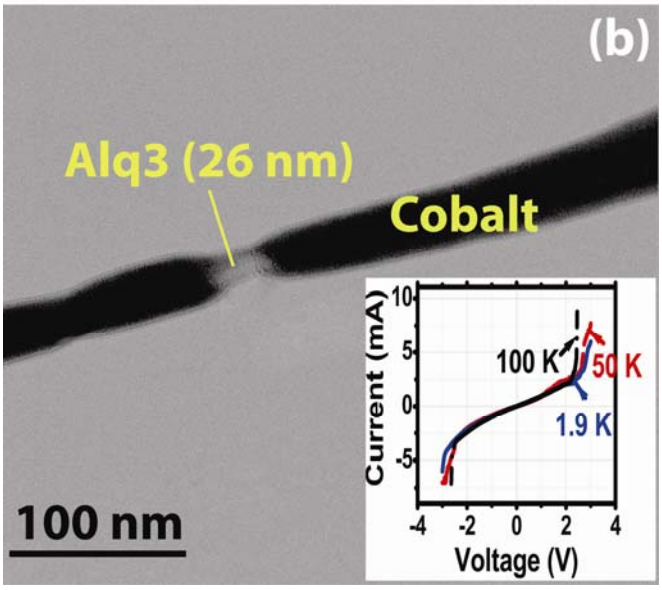

Fig. 1: A cross-section TEM of a nanowire organic spin valve with an organic (Alq_3) quantum dot of dimension 26 nm × 15 nm in the middle. This, and similar structures, were used to measure the T_1 time in the organic from spin valve measurements. The inset shows the measured current voltage characteristic of the spin valve at different temperatures.

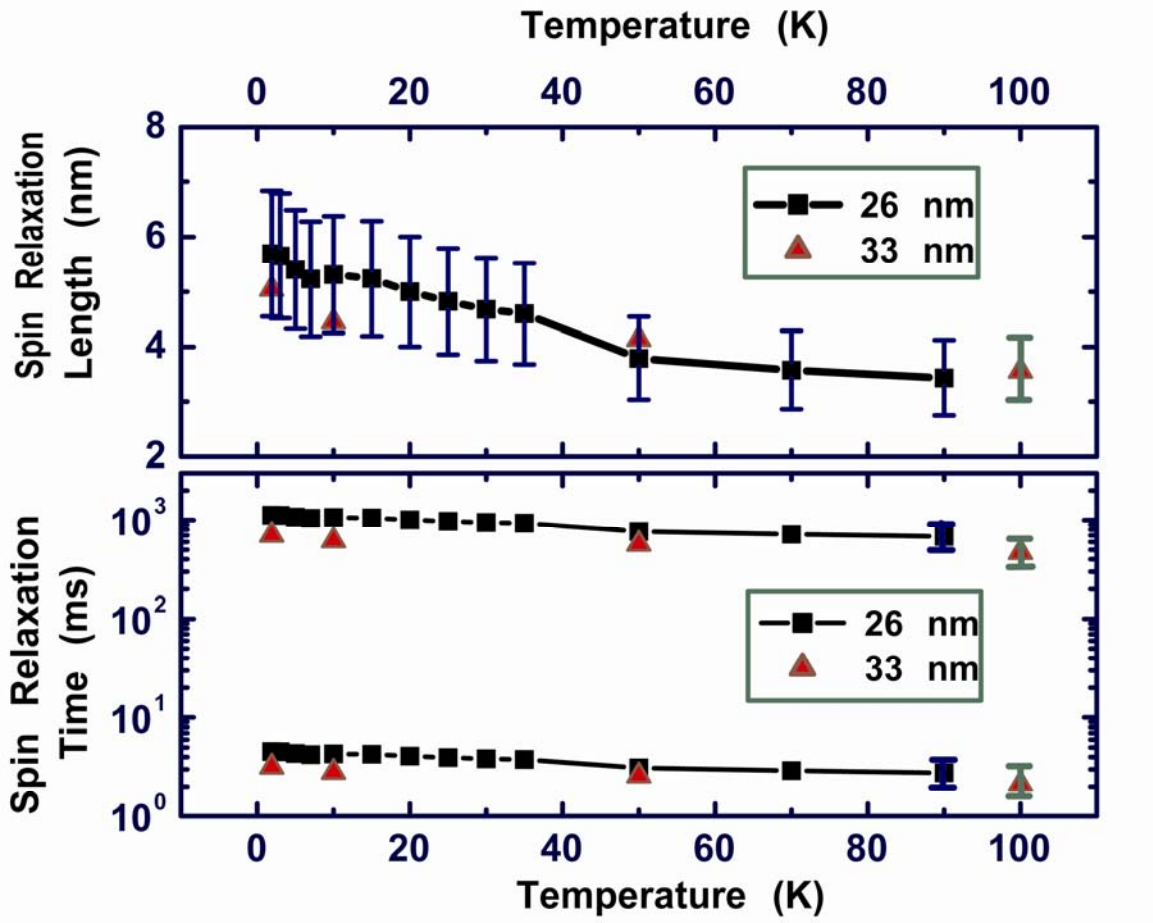

Fig. 2: The measured spin diffusion length (extracted from the spin valve peaks) and the spin relaxation time T_1 in Alq_3 "quantum dot" as a function of temperature.

T_2 time: We captured few molecules of *Alq_3* in "nanocracks" formed in anodized alumina films produced by anodizing Al in sulfuric acid. These cracks are 2-3 nm in diameter and since the Alq_3 molecule has a dimension of 0.8 nm, we can at most house 2-3 molecules in a nanocrack. Fig. 3 shows a high resolution FE-SEM micrograph showing a nanocrack. Capturing the molecules selectively in nanocracks involves a procedure that requires absorbing the molecules in pores followed by thorough rinsing in dichloro-ethane to remove the molecules from everywhere except the nanocracks.

We measured the transverse relaxation time T_2 in both bulk Alq_3 and few-molecule ensembles captured in the nanocracks using electron spin resonance spectroscopy (ESR) at various temperatures. A representative ESR spectrum is shown in Fig. 4. From the measured linewidth, which is nearly Lorentzian, we can estimate the T_2 time.

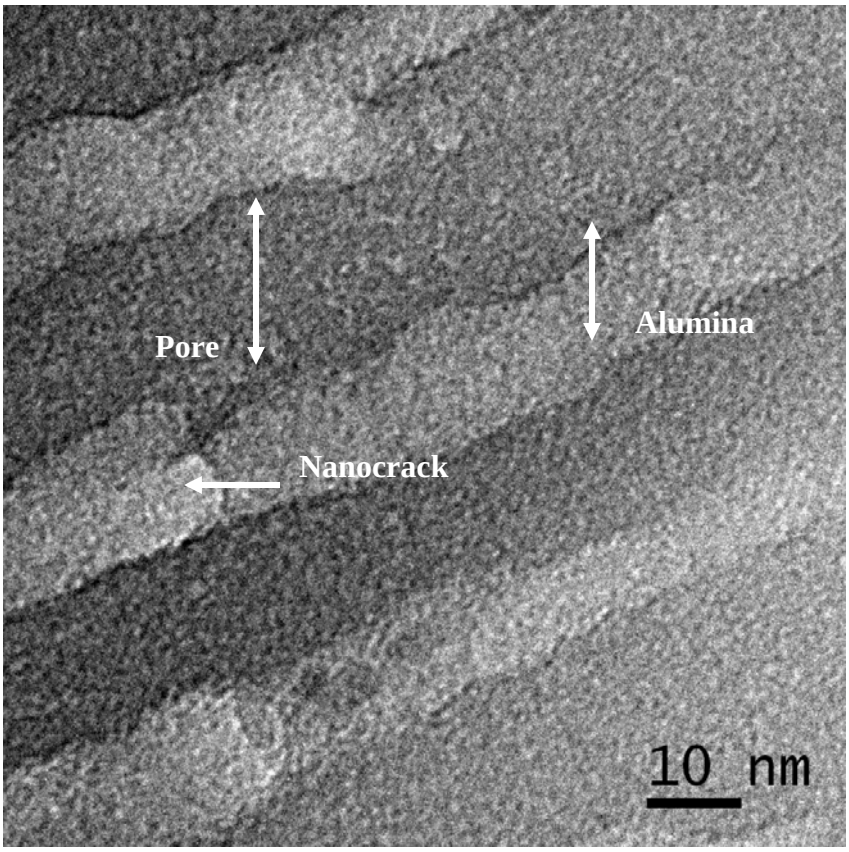

Fig. 3: Medium high resolution cross section FE-SEM micrograph of a nanocrack formed in porous alumina membranes.

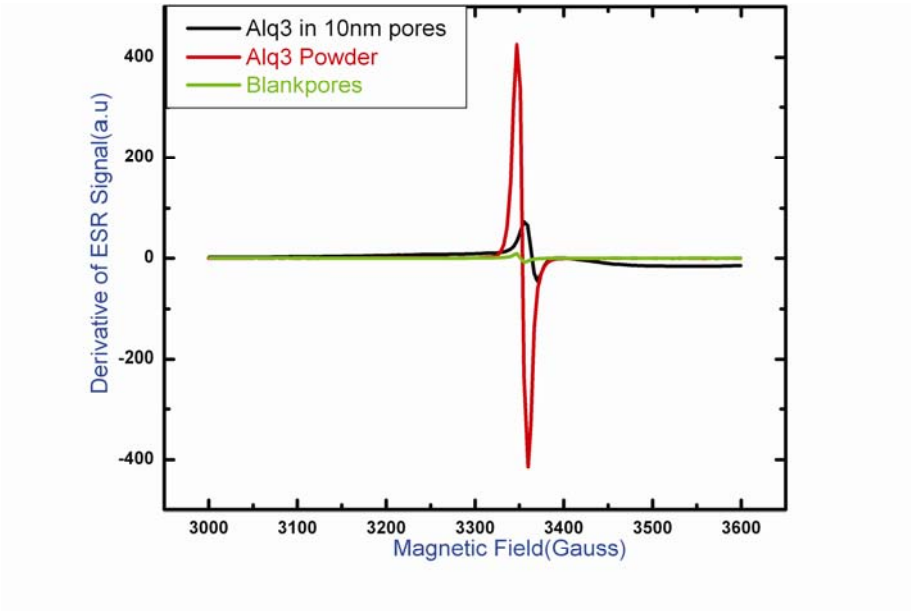

Fig. 4: ESR spectra of blank alumina, bulk Alq_3 powder and few-molecules of Alq_3 captured in nanocracks

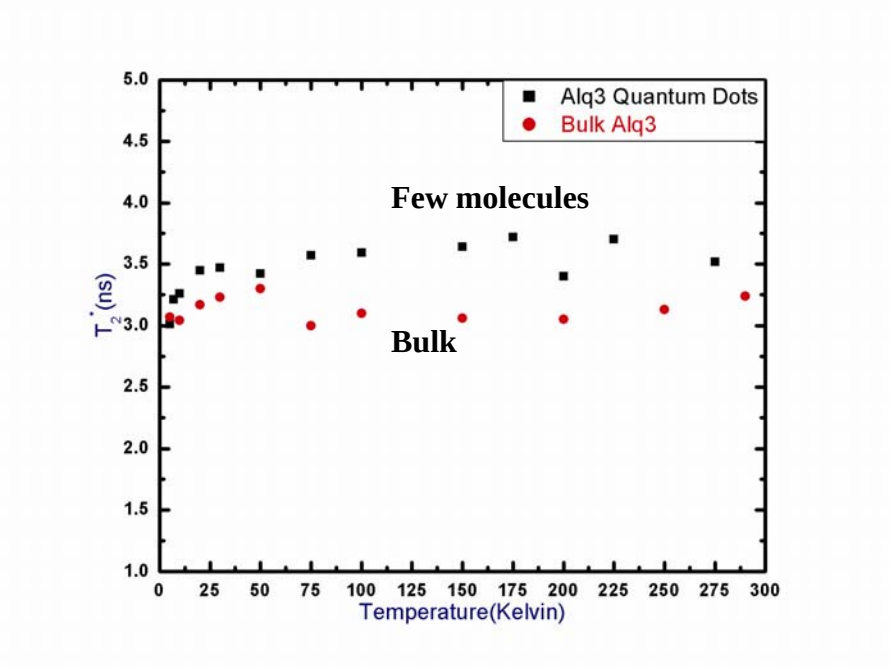

Fig. 5: Measured T_2 time (dephasing time) associated with delocalized spins in Alq_3. The dephasing time is relatively temperature independent. The few-molecule ensemble has a slightly higher T_2 time than the bulk sample.

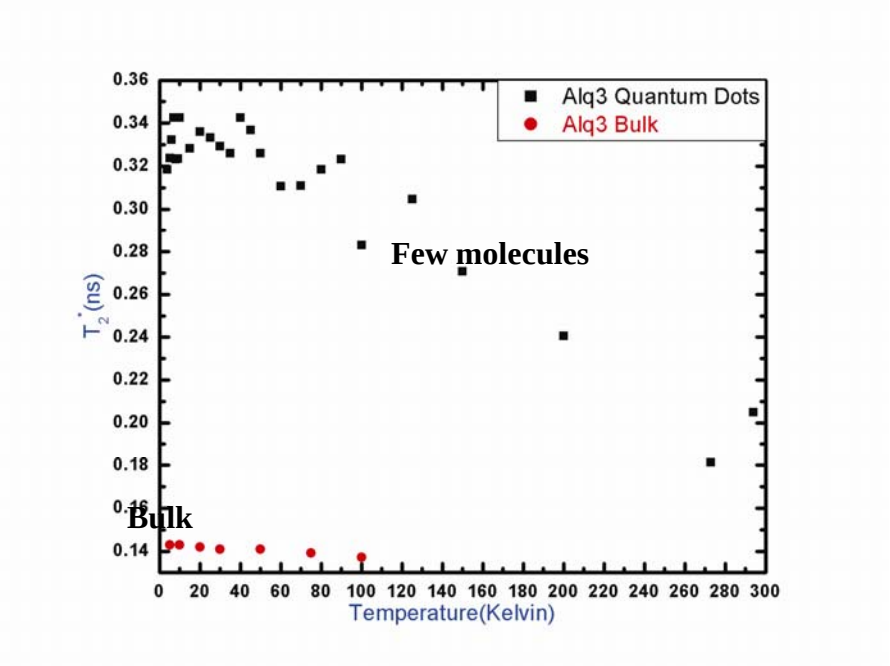

Fig. 6: Measured T_2 time (dephasing time) associated with localized spins localized at impurity sites in Alq_3. The dephasing time is temperature dependent. The few-molecule ensemble has a much higher T_2 time than the bulk sample.

We found that Alq_3 has two T_2 times – one associated with delocalized spins and the other with localized spins [2]. For the former, the primary dephasing mechanism is spin-spin interaction (which is why it is temperature independent) and for the latter, it is obviously spin-phonon interaction (which is why it is temperature dependent). We made several important observations:

1. The T_2 time associated with delocalized spins is long enough to satisfy the Knill criterion for fault-tolerant quantum computing [3].
2. The fact that the few molecule ensemble has a much higher T2 time than bulk in the case of localized spins which diphase through spin-phonon interaction is a strong evident for the phonon bottleneck effect in organic molecules. If true, this is the first evidence of the phonon bottleneck effect in organic molecules.

These observations have been reported in ref. [4].

Spin transport in organics

Spin transport in organic spin valves has some peculiarities that are not found in the case of inorganics. Consider the case of a spin valve made from Co, organic and Ni. Both Co and Ni have negative spin polarizations at the Fermi energy, meaning that the density of states of minority spins is actually higher at the Fermi energy than that of majority spins. The minority spins are carried by d-electrons while the majority spins are carried by s-electrons. At the Fermi level, the s- and d-electrons have *opposite* spins. Even though the d-electrons are more numerous at the Fermi energy (because of the higher density of states), they have heavier tunneling mass and are hence slower than the s-electrons. Therefore, we can selectively inject either s-electrons (with majority spins) or d-electrons (with minority spins) from the Co contact into an organic, provided we have a Schottky barrier of variable width at the interface. If the barrier is thin, then the more numerous d-electrons are preferentially injected, while if the barrier is thick, then the faster s-electrons are preferentially injected.

The transmission probability of s-electrons into the Ni contact is smaller than that of d-electrons since that latter have a higher density of states at the Fermi energy in Ni. Therefore, if we inject s-electrons from Co, then the resistance is higher when both contacts are magnetized parallel to each other compared to the situation when the contacts are magnetized anti-parallel to each other. If we inject d-electrons, then the situation is opposite. Therefore, if we carry out a spin valve experiment where we measure the magnetoresistance of a Co-organic-Ni structure, we expect to see a resistance peak between the coercive fields of Co and Ni if we inject d-electrons from Co. On the other hand, if we inject s-electrons, then we expect to see a resistance trough. Thus, depending on the width of the Schottky barrier at the interface, we will either see a peak (normal spin valve effect) or a trough (inverse spin valve effect).

We measured 90 samples where the Schottky barrier width (determined by interface states) varied randomly. As expected, we saw both resistance peaks and troughs. These data are shown in Fig. 7.
The insets of Figure 6 show the magnetoresistance traces for the highest normal and inverse spin valve signals that we have measured among all samples tested. In every sample, the spin valve

peak always occurs between the coercive fields of Ni nanowires (~800 Oe) and Co nanowires (~1800 Oe), as expected. Surprisingly, we found that the coercive fields do not vary significantly from sample to sample indicating that the variation of coercive fields between different nanowires, and therefore different samples, is extremely small. The magnetoresistances of the devices exhibiting the inverse spin valve effect typically saturate at low fields (0.2 Tesla in the figure shown), but those of devices exhibiting the normal spin valve effect tend to saturate at much higher fields.

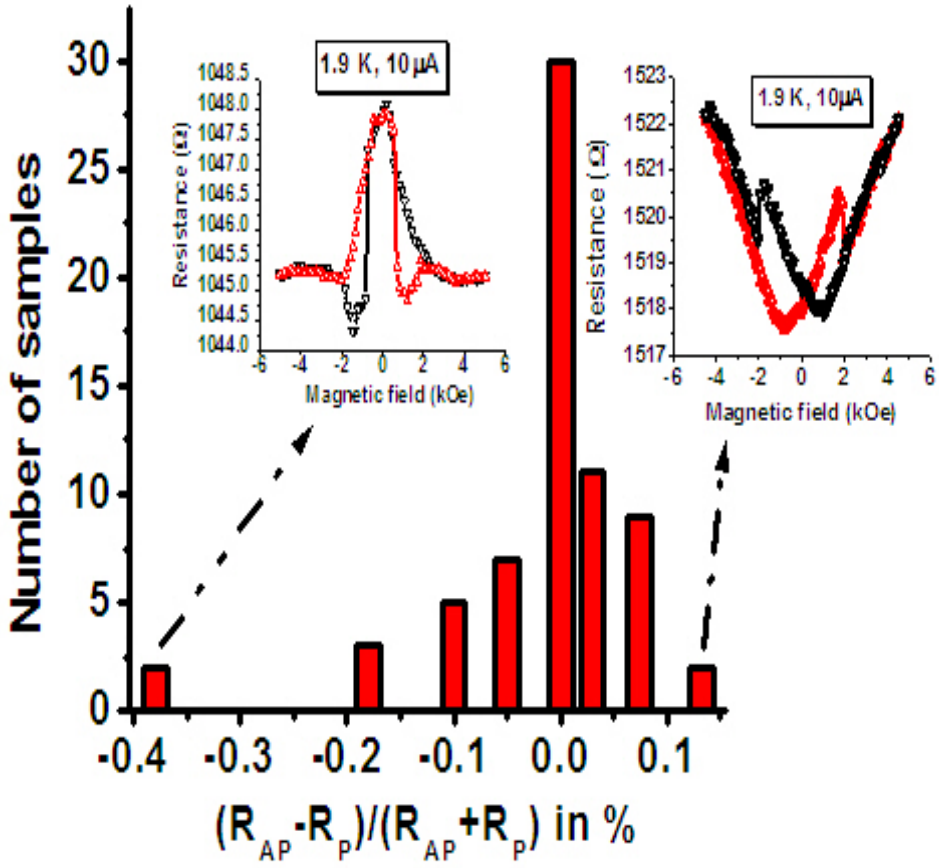

Fig. 7: Histogram showing the distribution of spin valve signal strength collected over 90 samples. Some of these samples show a positive spin valve signal and the rest a negative spin valve signal. All of these data were collected at a bias current of 10 μA rms. The insets show the magnetoresistance traces for two samples showing the inverse and the normal spin valve effect.

Figure 8 shows the magnetoresistance traces of a sample exhibiting a negative spin valve signal at four different temperatures. The bias current is kept constant at 10 μA rms. The spin valve signal decreases with increasing temperature indicating that the spin diffusion length in the organic decreases with increasing temperature.

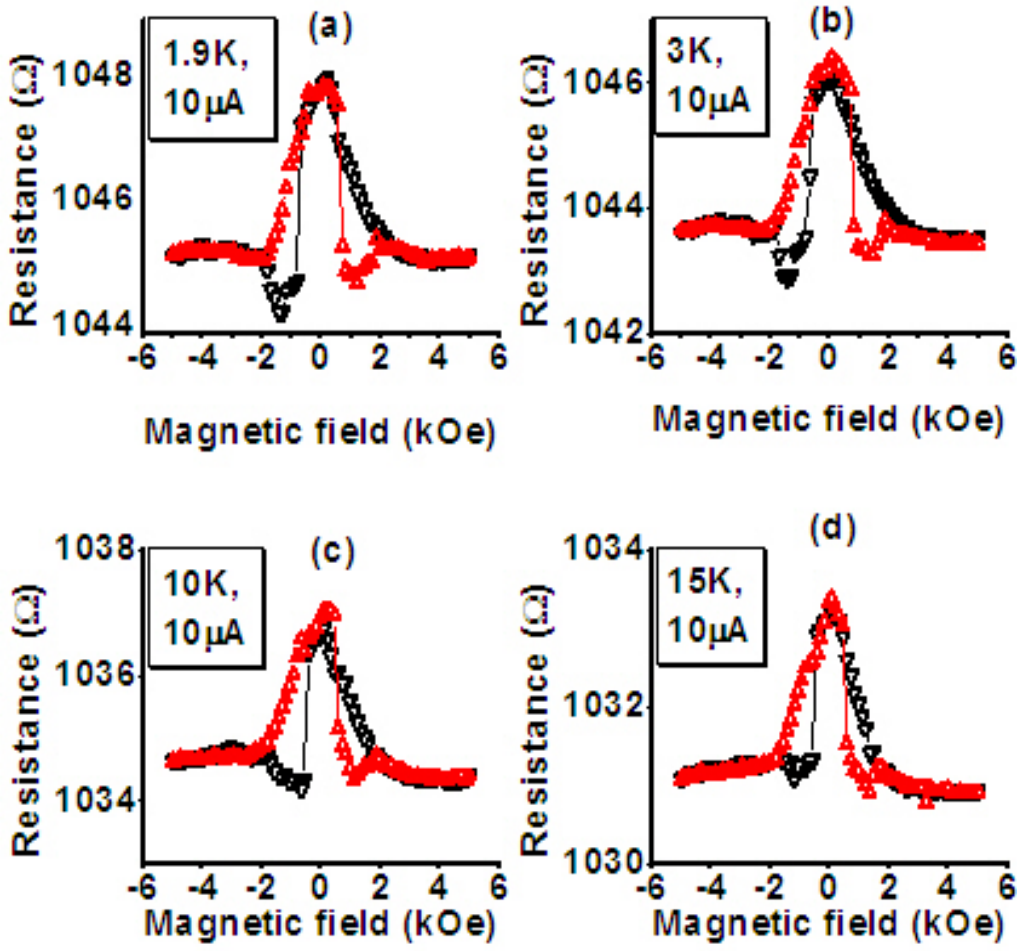

Fig. 8: Inverse spin valve effect and background negative magnetoresistance in Ni-Alq_3-Co nanowires at four different bias values and fixed temperature (1.9 K).

Figure 9 shows the bias current dependence of the negative spin valve signal in a typical sample at a constant temperature of 1.9 K. As the bias current is increased, the spin valve signal decays rapidly and at 200 μA rms, no signal is measurable with our apparatus. This happens because with increased bias current, there is increased carrier scattering which leads to more rapid spin relaxation and a shorter spin diffusion length. The spin valve signal has an inverse exponential dependence on the ratio of the device length to the spin diffusion length. As the latter decreases, the spin valve signal becomes increasingly smaller, and ultimately imperceptible. The high current however does not destroy the sample irreversibly. As the current is decreased, the spin valve signal is recovered.

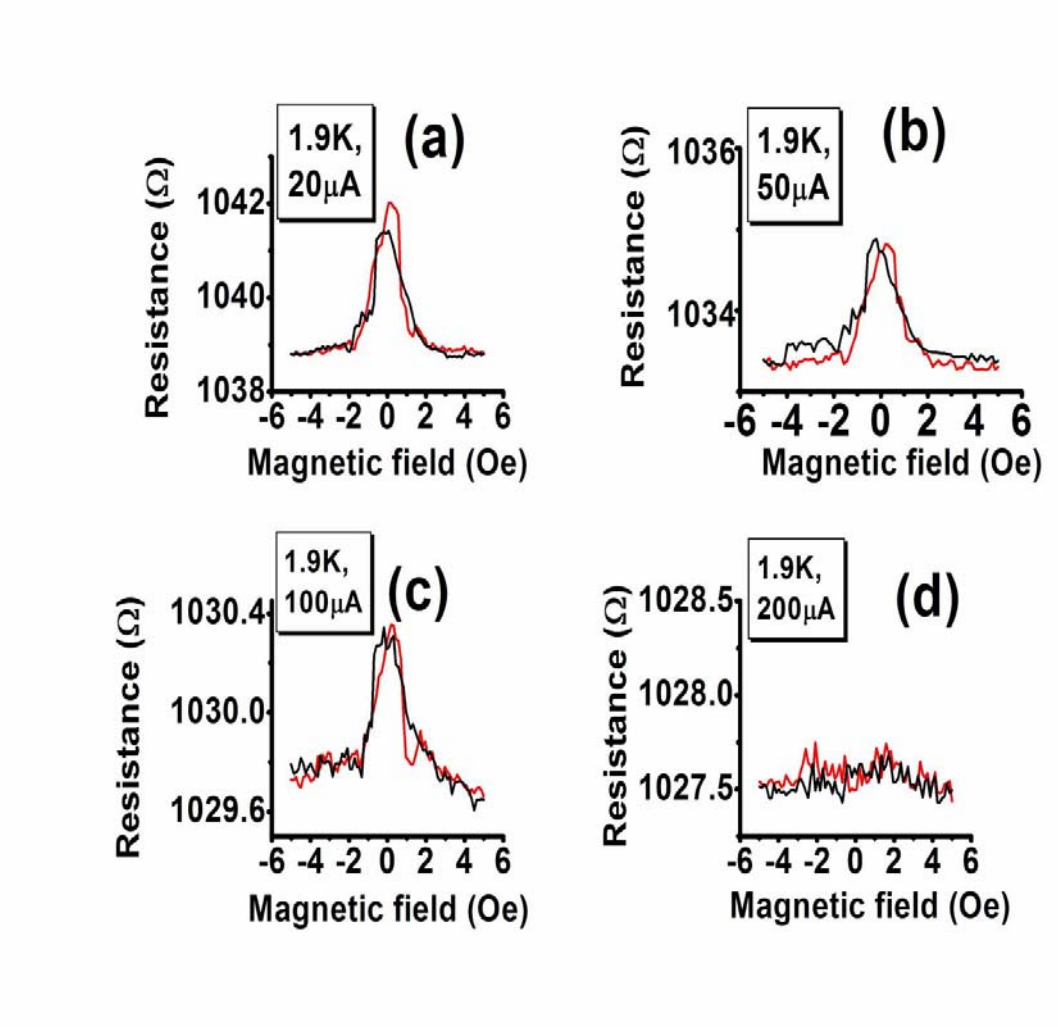

Fig. 9: Inverse spin valve effect and background negative magnetoresistance in Ni-Alq_3-Co nanowires at four different bias values and fixed temperature (1.9 K).

Figure 8 also shows that there is a background monotonic magnetoresistance δR ($|B|$) accompanying the spin valve signal and its sign is negative ($R(|B|) < R(0)$). We found consistently that whenever the spin valve signal is negative, the background magnetoresistance is also negative, and whenever the spin valve signal is positive, the background magnetoresistance is positive (see the insets of Figure 1). The background magnetoresistance has very little sensitivity to temperature (Figure 8), but it is extremely sensitive to bias, as can be seen in Figure 9. It disappears at a bias current of 200 μA.

Based on the above observations, we have formulated an explanation as to why a peak is accompanied by a positive background magnetoresistance and a trough is accompanied by a negative background magnetoresistance. At any magnetic field, except between the coercive fields of the two ferromagnets, the magnetizations of the injecting and detecting contacts are parallel. Now consider the case when the spin valve peak is positive (normal spin valve effect), meaning that the Schottky barrier at the Co/organic interface is narrow and we are injecting

primarily d-electrons. In this case, an injected carrier will transmit easily into Ni and contribute to current if its spin does not flip within the spacer layer. In the presence of spin orbit interaction, a magnetic field will increase the spin flip rate by inducing spin mixing. Thus, the probability of spin flipping increases with increasing magnetic field. If the injected carrier's spin flips, then it will be blocked by the detecting contact which has a larger density of states for d-electrons at the Fermi level and the current will decrease resulting in an increase in resistance. Thus, the resistance should increase with increasing magnetic field, resulting in a *positive* background monotonic resistance. This is what we observe.

In the case of negative spin valve signal (inverse spin valve effect), we are injecting s-electrons which have opposite spins as the d-electrons. In this case, spin flipping within the spacer layer will allow the flipped spin to transmit through the detector contact since the flipped spins have the same polarization as the d-electrons at the Fermi energy in Ni. Thus, spin flip events increase the current through the device and decrease the device resistance, instead of increasing it. Since a magnetic field increases the spin flip rate, the resistance will decrease with increasing magnetic field, resulting in a negative monotonic background resistance. Again, this is exactly what we observe.

Implications of these results for spin based quantum computing

The above result has serious implications for spin based quantum computing. It establishes that magnetic fields are extremely harmful since they reduce spin relaxation times. Most proposals for quantum computing advocate the use of strong magnetic fields for qubit initialization. Such magnetic fields can flip the spin and introduce high error rates. Thus, the use of a magnetic field in quantum gates can be counter-productive.

In contrast, our proposal for spintronic quantum gates [Phys. Rev. B, 61, 13801 (2000)] advocated the use of electrical spin control exercised via the Rashba interaction. Although the Rashba interaction can also cause some spin dephasing, it is not as disruptive as a magnetic field, particularly if organics are used as qubit hosts.

InAs dots for spintronics

InAs is a narrow gap semiconductor with a large g-factor (-15) and strong Rashba interaction. The large g-factor makes it possible to obtain large Zeeman splittings at relatively small magnetic fields. The strong Rashba interaction allows qubit rotations using moderate electric field strengths.

We have demonstrated the growth of InAs quantum dots (QDs) on straind GaAs. We used molecular beam epitaxy (MBE).

`InAs Quantum Dots Growth on GaAs Substrate:`

In the In(Ga)As/GaAs system QDs are grown in the Stranski-Krastnov (SK) mode. In this mode the mismatch between GaAs and In(Ga)As is initially accommodated by the compression of the initial InAs layer (wetting layer) preserving 2D growth. Since the lattice constant of InAs is greater than that of GaAs, the increase in the thickness of this layer results in an increase in the strain energy which makes development of heteroepitaxial islands [three dimensional (3D) growth] more favorable than 2D layer-by-layer growth. If one stops further growth of InAs at the time when transition from 2D growth to 3D growth takes place one obtains well defined partially strain-free and dislocation-free islands (QDs). We employed reflection high energy electron diffraction (RHEED) in our MBE system to track the changes from 2D growth to 3D growth. Figure 10 shows the changes in the RHEED pattern during InAs growth. Figure 11 (a) corresponds to 2D InAs growth whereas Fig. 11 (b) correspond to 3D growth of InAs, which indicates the formation of QDs.

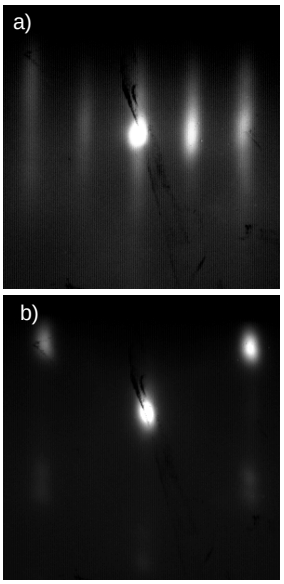

Fig. 10: RHEED pattern with beam in the [110] direction (a) 2×4 surface at the start of InAs (2D) growth, (b) spotty RHEED pattern after

The density and the size of the QDs are usually controlled by controlling the growth rates and InAs coverage. These parameters can also be controlled by growth temperature. High density and smaller size InAs QDs are obtained at lower temperatures. Another factor that plays an important role in QDs growth is the strain field, which causes the transition from 2D to 3D at a critical coverage of InAs. In some studies the QDs have been grown on strain field engineered GaAs or AlGaAs at a fixed substrate temperature. The effect of substrate temperature on the growth of QDs grown on strained GaAs has so far not been sufficiently studied.

We study the growth of InAs QDs on GaAs at different substrate temperatures with altered strain field in GaAs. The strain field was changed by introducing a 5.0 nm $In_{0.15}Ga_{0.85}As$ layer between a GaAs buffer layer (1.0μm) and a thin GaAs layer (2.0 nm) on which the InAs QDs were grown. As a result, QD density has been shown to be strongly dependent on temperature. This temperature dependence manifests itself by an increase in QD density at the rate of 9.0×10^{8} cm^{-2} per ºC decrease in temperature. Whereas the QD density directly grown on the GaAs decrease at the rate of 6.7×10^{7} cm^{-2} per ºC. The higher density QDs with smaller size (~3 nm height) are obtained by decreasing temperature and keeping growth rate and coverage constant. The growth of smaller quantum dots is favorable for vertical coupling (entanglement) of the quantum dots. Figure 11 shows the AFM images of the QDs grown at 510 ºC on GaAs substrate without [Fig. 11 (a)] and with [Fig. 11 (b)] an $In_{0.15}Ga_{0.85}As$ layer.

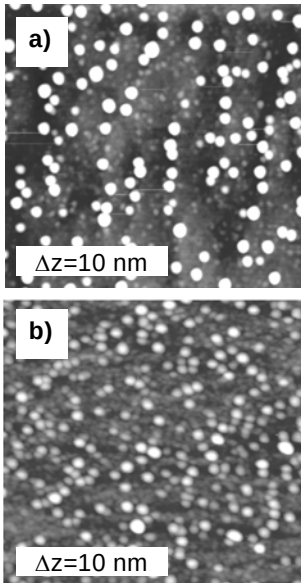

Fig. 11: $1\times1\mu m^2$ AFM images of QDs grown on GaAs at 510 ºC (a) without, and (b) with 5.0 nm $In_{0.15}Ga_{0.85}As$ layer.

The AFM images of the samples grown with the $In_{0.15}Ga_{0.85}As$ layer at substrate temperatures of 510 ºC, 485 ºC, and 465 ºC are shown in Fig. 12 a), b), and c) respectively. These images depict the effect of substrate temperature on the growth of QDs on the strain modified GaAs layer. The average densities of the QDs were 2.3×10^{10} cm^{-1}, 4.0×10^{10} cm^{-1}, and 6.6×10^{10} cm^{-1} when the growth temperatures of 510 ºC, 485 ºC, and 465 ºC were used, respectively. The QDs base to height aspect ratio decreased with the increase in the QDs growth temperature. Flatter and smaller QDs are obtained at lower growth temperatures. These smaller dots can be stacked with lower spacing between the QDs, which is required for the entanglement of the QDs wavefunctions. The amount of InAs (calculated from the dot's density and the base length) is $6.5\pm0.5\times10^{-5}$ grams per μm^2 for all cases, which is expected from the same transition time from 2D growth to 3D growth. Thus, we kept the InAs coverage constant in our study.

To measure the photoluminescence (PL) of InAs QDs we embedded the InAs quantum dots in the GaAs matrix. In Fig. 13, PL indicated by Sample B, Sample C, and Samples D correspond to QD images presented in Fig. 12 a, b, and c, respectively. The PL indicated by Sample A is corresponds to QD image presented in Fig. 6 a. As expected with a decrease in the size of the QDs the PL energy is increased due to increased confinement. For smaller QDs, the confinement in the GaAs matrix increases the energy of the conduction and decreases the energy of the valence band. Thus the difference in the energy which appears in the PL is higher for smaller QDs. We also observed that as the growth temperature of the QDs decreases the width of the PL energy also decreases. We correlate this observation with the reduction in the size distribution of the QDs. This size distribution is larger for larger quantum dots as compared to the smaller QDs. Since the laser excitation samples an area larger than 1μm, this size distribution appears in the PL line width. This line width can be reduced by different techniques which limit the excitation source to a lower number of QDs.

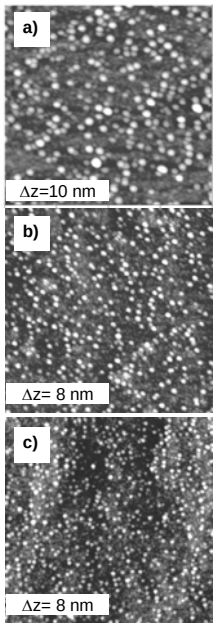

Fig. 12 1×1 μm^2 AFM images of QDs grown on GaAs with an $In_{0.15}Ga_{0.85}As$ layer at (a) 510 ºC, (b) 485 ºC, and (c) 465 ºC.

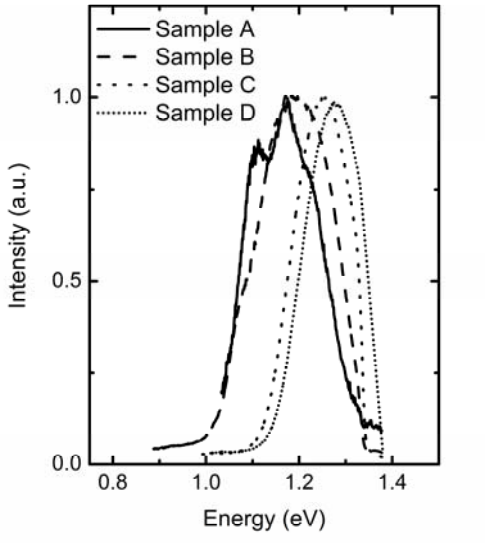

Fig. 13; PL from InAs QDs in the GaAs matrix grown (a) without an AlGaAs layer at 510 ºC, (b) with an $I_{0.15}Ga_{0.85}As$ layer at 510 ºC, (c) with an $I_{0.15}Ga_{0.85}As$ layer at 485 ºC, and (d) with an $I_{0.15}Ga_{0.85}As$ layer at 465 ºC.

Conclusion:

We successfully investigated the effect of temperature on the growth of InAs QDs grown on the stain modified GaAs layer. We observed that the QD grown with InGaAs layer have higher density and smaller size than the QD grown directly on the GaAs. Using this method we can grow smaller and flatter QDs which are favorable for vertical stacking with separation < 8nm which is required for entanglement of QDs states. The entanglement of the state is the basic requirement for realization of quantum computation.

ZnO nanostructures as possible qubit hosts.

ZnO has a wide gap and weak spin orbit interaction which makes it an attractive material host for spin based qubits. Research was carried out in the realm of both ZnO growth and self assembly of ZnO nanostructures.

ZnO Nanorods on Different Substrates:

We have studied the growth and properties of ZnO nanorods on Si, GaN/Sapphire and bulk ZnO. ZnO nanorods were grown by catalyst-assisted vapor phase transport on Si(001), GaN(0001)/*c*-Al_2O_3, and bulk ZnO(0001). A mixture of ZnO and C powder was used as the material source and placed in the high temperature zone of a horizontal furnace. The substrates were located downstream of an Ar carrier gas in a lower temperature zone, and the growth temperature was 600-650 ºC. Continuous and patterned gold films 2 to 5 nm thick served as a catalyst. The localized conductive behavior, morphology, and optical properties were studied by using conductive atomic force microscopy (C-AFM), secondary electron microscopy (SEM)/transmission electron microscopy (TEM), and photoluminescence (PL) respectively.

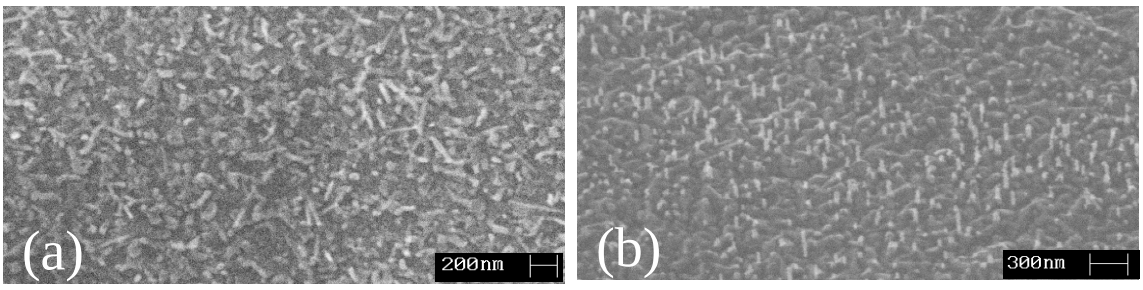

Fig. 9 SEM images of ZnO nanorods grown on (a) Si(001) and b) GaN/Al_2O_3 substrates.

Different morphologies were obtained for structures grown on different substrates. Nanorods of about 50 nm in diameter are vertically aligned on ZnO and GaN (along the c-axis of substrate), while they show large diameters (70-100 nm) and random orientation on Si(001). SEM images of ZnO nanorods grown on Si(001) and GaN(0001)/Al_2O_3 substrates are shown in Fig. 9. The morphology of ZnO nanorods grown on ZnO substrates is very similar to that of the rods grown on GaN. High-resolution TEM images (see Fig. 10) also show that ZnO nanocrystals nucleate on

Si(001) with c-axes oriented randomly in regard to the substrate. SEM studies revealed nanorods aligned in the direction perpendicular to the substrate surface for the samples grown on GaN/Al_2O_3 and ZnO substrates, while randomly oriented rods were observed on Si(001) substrates.

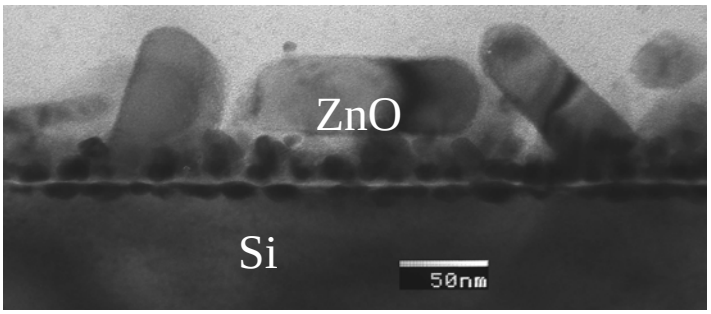

Fig. 15: Cross-sectional TEM image of ZnO nanorods grown on Si(001).

To study the localized conductive behavior using C-AFM, contacts were formed on all samples using indium solder, and a microscopic Schottky contact was formed between the metalized C-AFM tip and the sample. Data were acquired using a Veeco Dimension 3100 AFM with Ti/Pt-coated cantilevers and a current amplifier module with a range of 1 pA to 1 μA. During imaging contact-mode topography was acquired simultaneously with C-AFM current images. For I-V characterization, the sample bias was ramped from -12 to +12 V. C-AFM measurements revealed the rectifying behavior for ZnO rods grown on Si substrate. Figure 16 shows local I-V spectra for a single ZnO nanorod on Si

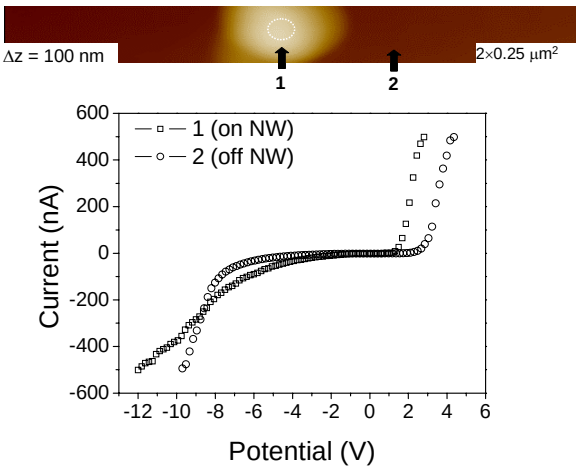

Fig. 16 Local I-V spectra taken from the top of a ZnO nanorod (curve 1) and of the nanorod (curve 2) using C-AFM on ZnO sample grown on Si(001) with a patterned gold film. Top panel presents contact-mode AFM images showing the points where the I-V spectra were recorded.

substrate measured by C-AFM. C-AFM measurements on samples grown on Si substrates with patterned Au films showed the absence of long-range in-plane conduction through ZnO nanorods indicating that nanorods are electrically isolated from each other.

Spectral structure and intensity of low-temperature PL from ZnO nanorods grown on Si are comparable to that from bulk ZnO (see Figure 17a). Band edge-to-deep emission ratio is about 4 orders of magnitude, slightly varying from sample to sample. Figure 17b shows excitonic

spectral range for ZnO grown on Si. 15-K PL spectra are dominated by donor bound exciton (DBX) lines. Depending on sample morphology, the peak position of dominating line varies from 3.353 to 3.355 eV. Similar peak positions were frequently reported for ZnO nanorods grown by vapor transport and CVD methods

Variation in PL-line positions can be attributed to strain. Biaxial compressive stress with magnitude varying from sample to sample was found from Raman measurements for the samples grown on Si. However, relationship between the microstructure of samples and stress needs further investigations. The full width at half maximum of the DBX line ranges from 5 to 7 meV and its phonon replicas are clearly visible for the samples grown on Si. PL spectra for ZnO rods grown on Si and GaN are qualitatively similar (see Figure 12c). For nanorods grown on ZnO substrates, the identification of the lines related to nanorods was impossible due to spectral overlap with the PL from bulk ZnO. We also observed the stimulated emission in ZnO nanorods grown on GaN/sapphire substrate. Time resolved PL measurements show the decay constants for all nanorod samples are much higher than typical values for ZnO thin films grown by RF sputtering on sapphire, and approach those for a ZnO/Al_2O_3 sample grown by molecular beam epitaxy (MBE), indicating rather high crystal quality of the material.

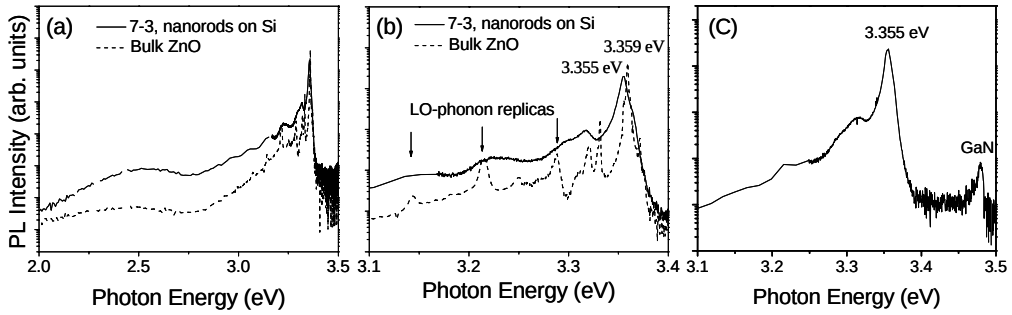

Fig. 17: 15-K PL spectra of ZnO nanorods grown on (a), (b) Si(001) and (c) GaN/Al_2O_3. (a) Wide spectral range and (b) excitonic range.

Conclusion:

ZnO nanorods were grown by catalyst-assisted vapor transport on Si(001), GaN(0001)/*c*-Al_2O_3, and bulk ZnO(0001). Morphology of the ZnO nanostructures grown on Si differs drastically from those on GaN and ZnO. Nanorods are vertically aligned on ZnO and GaN substrates, while they exhibit random orientation on Si(001). Conductive AFM measurements show rectifying behavior of I-V characteristics for ZnO nanorods grown on Si substrate. Low temperature (15-K) PL spectra are dominated by donor-bound exciton lines around 3.355 eV with a FWHM of 5-7 meV. PL decay times measured by time-resolved PL vary from 0.14 ns for the nanorods on GaN/ Al_2O_3 to 0.26 ns on Si. Stimulated emission was observed for nanorods grown on GaN/ Al_2O_3, most likely, due to their better vertical alignment compared to Si substrates.

ZnO nanowires electrochemically self assembled

ZnO nanowires were electrochemically self assembled prepared as follows. A 99.997% pure Al foil was degreased and electropolished in a solution of perchloric acid, butyl cellusolve, ethanol and distilled water to produce a mirror like surface. This film was then washed in distilled water, air dried and anodized in 3% oxalic acid at room temperature using a constant anodizing voltage of 40 V. The anodization was carried out for several hours to form a thick porous alumina film on the surface. This film was stripped off in hot chromic/phosphoric acid and the anodization repeated again for 5 minutes to form another porous alumina film of thickness less than 1 μm. The two-step anodization process yielded an anodic alumina film with a well ordered array of 50 nm diameter pores.

The pores were then selectively filled up with Zn using ac electrodeposition in a non-aqueous solution. The solution consisted of $ZnClO_4$ (10.5 gm), $LiClO_4$ (2.5 gm) and dimethyl sulfoxide (250 ml). The porous film was immersed in the solution and an ac potential of 25 V rms and frequency 250 Hz was imposed between the aluminum substrate and a graphite counter electrode. The temperature was maintained at 75^{o} C. During the negative cycle of the ac voltage, the Zn^{++} ions in solution were reduced to zero-valent Zn atoms which were selectively electrodeposited within the pores since they offered the least impedance path for the ac current (displacement current) to flow. During the positive ac cycle, the Zn atoms were not oxidized back to Zn^{++} ions since alumina is a valve metal oxide. Metallic Zn within the pores was then oxidized to ZnO by immersion in H_2O_2 at room temperature for 5 hours. This method is slightly different from the technique employed in the literature. A TEM image of an isolated ZnO nanowire synthesized by our technique is shown in Fig. 18.

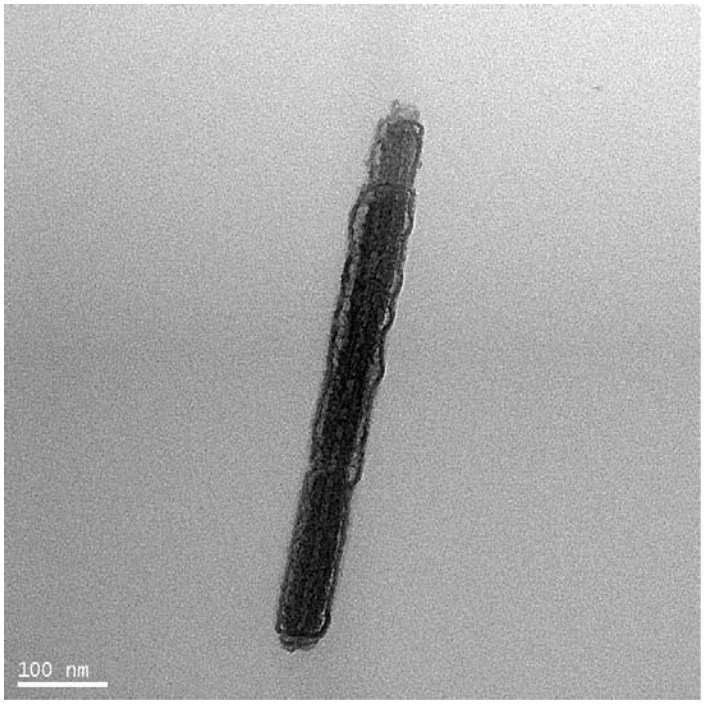

Fig. 18: TEM image of a single released ZnO nanowire of 50 nm diameter.

For PL measurement, the samples were excited by coupling a 50mW HeCd laser emitting at 325nm to an UV-LabRamHR micro-PL/Raman system from Jobyn-Yvon and the luminescence detected with a LN_2 cooled CCD detector. The spot size of the exciting beam was 10 μm in diameter and the excitation beam was normally incident on the sample surface. The small spot size revealed that there is significant inhomogeneity in the samples on the size scale of 10 μm. Some regions of the sample do not luminesce well and do not show any phonon replicas, while some other regions luminesce brightly and show numerous phonon replicas. We believe that this inhomogeneity accrues from the randomness of interface states and defects. Some regions have more interface states and defects that provide a route for non-radiative recombination of photo-excited carriers, which quench the PL, while other regions are relatively defect free and show bright PL. If we use a large spot size (2 mm) to illuminate the sample, then we do not observe the phonon replicas because of ensemble averaging over many regions that are highly defective. In Fig. 14(a) and 14(b), we show the PL spectra of two samples collected from ~ 10 μm regions that show bright luminescence and phonon replicas.

The PL spectra in Fig. 19 show a high frequency peak centered at 370 nm wavelength (energy = 3.31 eV) which is about 60 meV below the room temperature bandgap of bulk ZnO (3.37 eV). Since the exciton binding energy in ZnO is ~ 60 meV, we assign this peak to exciton recombination. Note that the size of the nanowires is too large to show any blue shift in the PL due to quantum confinement.

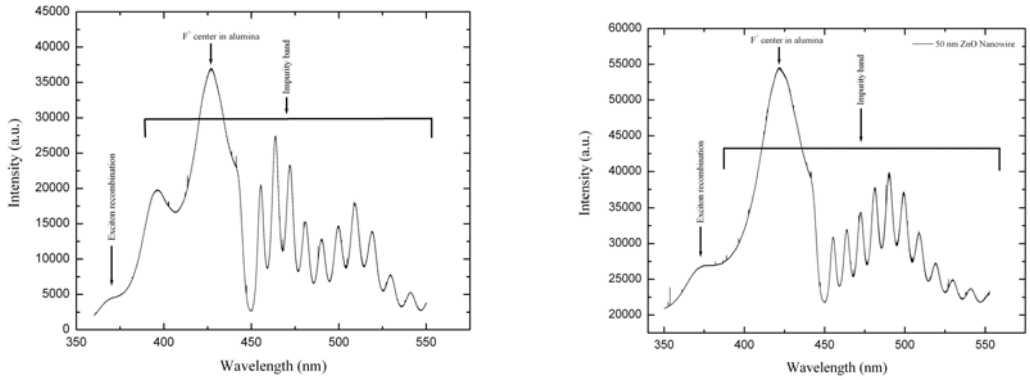

Fig. 19: PL spectra of ZnO nanowires showing numerous phonon replica peaks. The energy separation between neighboring peaks is 54 meV which corresponds to the non-polar high frequency E_2 phonon in ZnO. Different peaks are labeled to elucidate their origin. The spectra from two different samples are shown. The excitation spot size is 10 μm.

There is a broader peak centered at a wavelength of 430 nm. This peak, which has the highest intensity, is not related to ZnO, but is due to optical transitions in singly ionized oxygen vacancies (F^+ centers) in the alumina host and its origin has been confirmed by electron paramagnetic resonance measurements in the past Unfortunately, this peak masks some of the phonon replicas.

The phonon replicas, however, are easily discernible. The associated peaks are equally spaced in energy with an interval of 54 meV. ZnO has a number of phonon modes. Because bulk ZnO typically has a wurtzite crystal structure, the frequencies of both longitudinal optical (LO) and transverse optical (TO) phonon modes are split into two frequencies with symmetry A_1 and E_1. In addition, there are two non-polar phonons with symmetry E_2. The low frequency E_2 mode is associated with vibrations of the Zn sub-lattice and the high frequency E_2 mode is caused by vibration of oxygen atoms.

The high frequency E_2 phonon has an energy of 54 meV which matches the energy spacing between the peaks we observe. Therefore, we ascribe the phonon replicas to transitions involving this phonon. Normally, one observes phonon replicas associated with polar LO phonons in ZnO. Phonon replicas associated with the non-polar E_2 phonon has never been observed before, and to our knowledge, no observation of phonon replicas have been reported in ZnO *nanostructures*.

Phonon replicas appear in PL spectra when photogenerated electrons and holes (or excitons) recombine by simultaneous emission of phonons and photons. The excited electron first emits one or more phonons to decay to a lower energy level, and from there it emits a photon to decay to the valence band and recombine with a hole. The initial phonon emissions require that the electrons couple strongly with phonons. Since ZnO is a polar material, we expect the Fröhlich coupling with polar LO phonons to be particularly strong. However, we find that at least in the nanowires, the photogenerated carriers interact more strongly with the non-polar E_2 phonon via deformation potential coupling. This is a surprising result that needs further theoretical exposition.

The data in Fig. 19 also show that the n-phonon peak ($n \neq 0$) is more intense than the zero-phonon peak. One possible explanation for this odd behavior is a resonance effect. Resonant enhancement of phonon replicas have been observed before in quantum dots. It is possible that the deep levels in the ZnO nanowires, which are responsible for the green emission band, merge to form an impurity band in the bandgap. The electron first decays non-radiatively to this band by emitting one or more E_2 phonons and then decays to the valence band radiatively to recombine with a hole. If the efficiency of radiative recombination from certain states in the impurity band exceeds that of the direct exciton recombination, then we will expect the n-phonon peak ($n \neq 0$) associated with these “high efficiency states” to be more intense than the zero phonon peak. This situation is illustrated in Fig. 20.

In conclusion, we have observed numerous phonon replicas in the PL spectrum of ZnO nanowires which are associated with the high frequency non-polar E_2 phonon mode caused by vibration of oxygen atoms. Our results show that there is strong deformation potential coupling between photoexcited electrons and non-polar E_2 phonon modes in ZnO nanowires, even though ZnO is a strongly polar material. This is an unusual result that can shed new light on the nature of electron-phonon coupling in nanostructures.

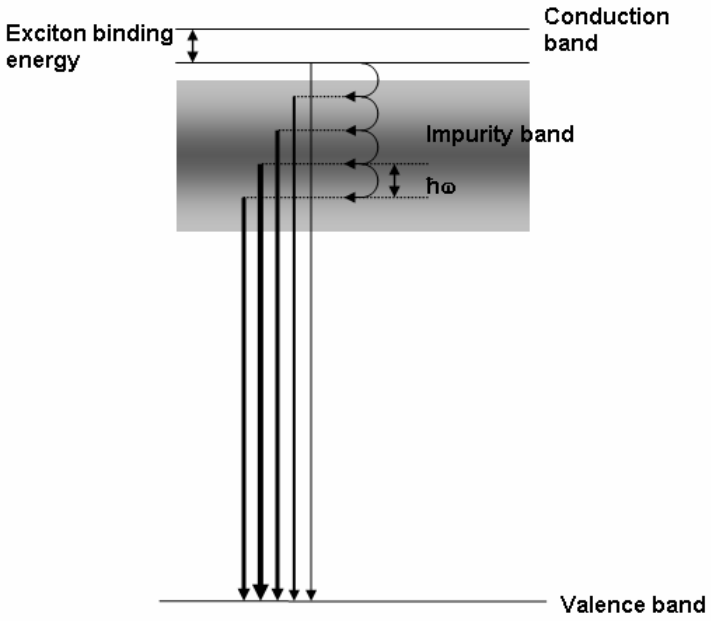

Fig. 20: Energy diagram explaining why the n-phonon peak can be more intense than the zero-phonon peak. The quantity ħω is the energy of the E_2 phonon. The vertical straight arrows indicate radiative recombination processes and the curved arrows indicate non-radiative phonon-assisted decay. The thicknesses of the straight arrows correlate with the efficiencies of the corresponding radiative recombination process.

Mn clusters are possible hosts for spin qubits

We investigated the magnetic properties of Mn_5 and Mn_6 clusters to investigate the magnetic moment and the effect of spin canting. The studies included the investigation of both collinear and non-collinear arrangements. It was shown that while the atomic structure of the ground state of Mn_5 is a triangular bipyramid, the collinear and non-collinear arrangements have comparable energies and hence are degenerate. For Mn_6, while the ground state has a square bipyramid arrangement, the non-collinear configuration is most stable making it the smallest cluster to feature a non-collinear ground state. The results were discussed in view of the recent experimental Stern-Gerlach profiles.

Personnel supported:

Faculty

1. Supriyo Bandyopadhyay
2. Alison Baski
3. Shiv Khanna
4. Hadis Morkoc

Post doctoral associates

1. Carmen Stefanita
2. Ifthikar Ahmed
3. V. Avrutin
4. U Ozgur
5. T. Morisato (visiting from Japan)
6. M. Qian
7. A. Reber

Graduate students

1) S. Pramanik (Received Ph.D. in December 2006. Currently Assistant Professor (tenure track) at Department of Electrical Engineering, University of Alberta, Edmonton, Canada)
2) B. Kanchibotla (expected to receive Ph.D. in June 2008)
3) J. Chris Moore (Received Ph.D. in December 2007. Currently Assistant Professor in Longwood University, VA).
4) Sridhar Patibandla (expected to received Ph.D. in June 2008)
5) Xiang Feng (continuing student).

Undergraduate students

I. D. Edmonds
II. C. Tomlin
III. P. Clayborne

Publications:

Review articles

1. S. Bandyopadhyay, "Self Assembling Quantum Dots and Wires", *Encyclopedia of Nanoscience and Nanotechnology*, Eds. James. A. Schwartz, Cristian Contescu and Karol Putyera, Marcel-Dekker, New York, (2004).
2. C. G. Stefanita, F. Yun, H. Morkoc and S. Bandyopadhyay, "Self assembled quantum structures using porous alumina on silicon substrates", *Recent Research Developments in Physics*, Vol. 5, 703-720 (Transworld Research Network, Trivandram, India, 2004).
3. S. Bandyopadhyay and M. Cahay, "Spin Field Effect Transistors", in *Handbook of Nanoscience Engineering and Technology*, Eds. William A. Goddard, III, Donald W. Brenner, Sergey E. Lyshevski and Gerlad J. Iafrate, Chapter 8 (Taylor and Francis, New York, 2007).
4. C. G. Stefanita, F. Yun, M. Namkung, H. Morkoc and S. Bandyopadhyay, "Many Faces of Nanotechnology: A Brief Review of Some Routes to Nanosynthesis and Applications", in *Handbook of Electrochemical Nanotechnology,* Eds. Yuehu Lin and Hari Singh Nalwa, Chapter 1, (American Scientific Publishers, Stevenson Ranch, CA, 2007).
5. M. Cahay and S. Bandyopadhyay, "Spintronics", in *Recent Advances in Silicon Nanotechnology*, Ed. Nobu Koshida, Springer Verlag, Berlin. Expected publication in 2008.
6. B. Kanchibotla, S. Pramanik and S. Bandyopadhyay, "Self Assembly of Nanostructures Using Nanoporous Alumina Templates", in *Handbook of Nano and Molecular Electronics*, Ed. E. Lyshevski, (CRC Press, 2007), Chapter 9.
7. S. Bandyopadhyay and M. Cahay, "Hybrid and monolithic spintronics", in *Information Technology*, Vol. II, Ed. R. Waser, Wiley-VCH, Germany. Expected publication in 2008.
8. S. Pramanik, B. Kanchibotla and S. Bandyopadhyay, "Device applications of electrochemically self assembled nanostructures", in *Handbook of Nanoscience and Nanotechnology*, 2nd edition, American Scientific Publishers, Stevenson Ranch, CA, (2008).
9. B. Kanchibotla, S. Pramanik and S. Bandyopadhyay, "Organic nano-spintronics", in *Handbook of Nanophysics*, Ed. D. Sattler, CRC Press. Expected publication date 2009.

Journal

1. M. Cahay and S. Bandyopadhyay, "Phase coherent quantum mechanical spin transport in a weakly disordered quasi one-dimensional channel", Phys. Rev. B., 69, 045303 (2004).
2. S. Pramanik, S. Bandyopadhyay and M. Cahay, "Decay of Spin Polarized Hot Carrier Current in a Spin Valve Structure", Appl. Phys. Lett., 84, 266 (2004).
3. C. G. Stefanita, S. Pramanik, A. Banerjee, M. Sievert, A. Baski and S. Bandyopadhyay, "Electrochemically Self Assembled Nanostructure Arrays", J. Crystal. Growth, 268, 342-345 (2004).
4. S. Bandyopadhyay, S. Pramanik and M. Cahay, "Spin Eigenenergies of Magneto-Electric Subbands in a Quantum Wire", Superlattices and Microstructures, 35, 67-75 (2004).
5. S. Bandyopadhyay and M. Cahay, "Another Spintronic Analog of the Electro-Optic Modulator", Appl. Phys. Lett., 85, 1814 (2004).

6. S. Bandyopadhyay and M. Cahay, “Re-examination of some spintronic field effect transistor concepts”, Appl. Phys. Lett., 85, 1433 (2004).
7. S. Bandyopadhyay and M. Cahay, “A Spin Field Effect Transistor with Low Leakage Current”, Physica E, 25, 399 (2004).
8. S. Bandyopadhyay, “Computing with Spins: From Classical to Quantum Computing”, Superlattices and Microstructures, 37, 77 (2005).
9. S. Pramanik, S. Bandyopadhyay and M. Cahay, “Spin relaxation in the channel of a Spin Field Effect Transistor”, IEEE Trans. Nanotech., 4, 2 (2005).
10. S. Bandyopadhyay and M. Cahay, “Proposal for a spintronic femto-Tesla magnetic field sensor”, Physica E, 27, 98-103 (2005).
11. S. Bandyopadhyay and M. Cahay, “Are spin junction transistors suitable for signal processing?”, Appl. Phys. Lett., 86, 133502 (2005).
12. S. Pramanik, S. Bandyopadhyay and M. Cahay, “Spin relaxation of ‘upstream’ electrons in a quantum wire: Failure of the drift diffusion model”, Phys. Rev. B., 73, 125309 (2006).
13. T. Basu, S. Sarkar and S. Bandyopadhyay, “Single spin logic circuits”, Phys. Low Dim. Struct., 2, 69 (2006).
14. S. Patibandla, S. Pramanik, G. C. Tepper and S. Bandyopadhyay, “Spin valve effect in Germanium nanowires”, J. Appl. Phys., 100, 044303 (2006).
15. S. Pramanik, C-G Stefanita and S. Bandyopadhyay, “Spin transport in an all metal spin valve: A study of the pure Elliott-Yafet mechanism”, J. Nanosci. Nanotech., 6, 1973 (2006).
16. J. Wan, M. Cahay and S. Bandyopadhyay, “Can a non-ideal metallic ferromagnet inject spin into a semiconductor with 100% efficiency without a tunnel barrier?”J. Nanoelectron. Optoelectron., 1, 62 (2006).
17. S. Ramanathan, S. Bandyopadhyay, J. D. Edwards and J. Anderson, “Fluorescence and infrared spectroscopy of electrochemically self assembled ZnO nanowires: Evidence of the quantum confined Stark effect”, J. Mat. Sci: Electron. Mater., 17, 651 (2006) (invited).
18. S. Ramanathan. L. K. Hussey, M. Munoz and S. Bandyopadhyay, “Observation of numerous E_2 mode phonon replicas in the room temperature photoluminescence spectra of ZnO nanowires: Evidence of strong electron-non-polar phonon coupling”, Appl. Phys. Lett., 89, 143121 (2006).
19. S. Pramanik, S. Bandyopadhyay, K. Garre and M. Cahay, “Positive and negative spin valve peaks and the background magnetoresistance in nanowire organic spin valves", Phys. Rev. B, 74, 235329 (2006).
20. S. Bandyopadhyay, “Power dissipation in spintronic devices: A general perspective", J. Nanosci. Nanotech., 7, 168 (2007).
21. S. Pramanik, C-G Stefanita, S. Bandyopadhyay, N. Harth, K. Garre and M. Cahay, “Observation of extremely long spin relaxation time in an organic nanowire spin valve”, Nature Nanotechnology, 2, 216 (2007).
22. T. Basu, S. Sarkar and S. Bandyopadhyay, “Design of a single spin arithmetic logic unit”, IET Circuits, Devices and Systems: Special Isssue on Quantum Dots, 1, 194 (2007).
23. J. Wan, M. Cahay and S. Bandyopadhyay, “A digital switch and femto-Tesla magnetic field sensor based on Fano resonance in a spin field effect transistor”, J. Appl. Phys., 102, 034301 (2007).

24. S. Pramanik, S. Bandyopadhyay and M. Cahay, "Energy dispersion relations of spin split subbands and gate control of spin polarization in a quantum wire", Phys. Rev. B., 76, 155325 (2007).
25. J. Wan, M. Cahay and S. Bandyopadhyay, "Spin Injection Transistor", IEEE Trans. Nanotech. , 7, 34 (2008).
26. H. Agarwal, S. Pramanik and S. Bandyopadhyay, "Single spin universal Boolean logic gate", New Journal of Physics (Focus Issue on Spin in Reduced Dimensions), 10, 015001 (2008).
27. P. Upadhayay, S. Pramanik, S. Bandyopadhyay and M. Cahay, "Magnetic field control of spin texturing in semiconductor quantum wires", Phys. Rev. B, 77, 045306 (2008).
28. S. Bandyopadhyay, "Single spin logic: Perpetuating Moore's law", Nanotechnology Perceptions, March 2008 (Invited by the editor Graham Holt).
29. J. Wan, M. Cahay and S. Bandyopadhyay, "A dual gate Spin Field Effect Transistor with low switching voltage and large conductance ON to OFF ratio", Physica E (in press).
30. A. Trivedi and S. Bandyopadhyay, "Dependence of the conductance ON/OFF ratio and transconductance of a Spin Field Effect Transistor on the spin injection efficiency", IET Circuits, Devices and Systems, 1, 395 (2008).
31. "Investigation of charge trapping at the oxide/semiconductor interface for MBE-grown GaN films," J.C. Moore, M.A. Reshchikov, J.E. Ortiz, J. Xie, H. Morkoç, A.A. Baski, *Gallium Nitride Materials and Devices III (Ed. H. Morkoç et al.), Proc. of SPIE* 6894, 68940B1-9 (2008).
32. "AFM and CAFM studies of ELO GaN films," V. Kasliwal, J.C. Moore, X. Ni, H. Morkoç, A.A. Baski, *Gallium Nitride Materials and Devices II (Ed. H. Morkoç* & *C.W. Litton), Proc. of SPIE* 6473, 647308 (2007).
33. "Local electronic and optical behavior of a-plane GaN grown via epitaxial lateral overgrowth," J.C. Moore, V. Kasliwal, A.A. Baski, X. Ni, Ü. Özgür, H. Morkoç, *Appl. Phys. Lett.* 90, 011913 (2007).
34. "Effect of temperature on the growth of InAs/GaAs quantum dots grown on a strained GaAs layer," I. Ahmad, V. Avrutin, H. Morkoç, J. C. Moore, A.A. Baski, *J. of Nanoscience and Nanotechnology* 7, 1–5 (2007).
35. "Study of leakage defects on GaN films by conductive atomic force microscopy," J.C. Moore, J.E. Ortiz, J. Xie, H. Morkoç, A.A. Baski, *J. of Physics: Conf. Series*: 61, 90-94 (2007).
36. "Comparative study of the (0001) and (000$\underline{1}$) surfaces of ZnO," S.A. Chevtchenko, J.C. Moore, Ü. Özgür, X. Gu, A.A. Baski, H. Morkoç, *Appl. Phys. Lett.*, 89, 182111 (2006).

Refereed Conferences

1. S. Pramanik, S. Bandyopadhyay and M. Cahay, "Why is the Spin Transistor Elusive?" IEEE NANO 2004, Munich, Germany, August 2004.
2. S. Pramanik, S. Bandyopadhyay and M. Cahay, "Monte Carlo simulation of spin transport in nanowires", IEEE NTC Workshop on Quantum Device and Technology, Clarkson University, Pottsdam, NY, May 2004.

3. M. Cahay and S. Bandyopadhyay, “Issues pertaining to spin injection across ferromagnetic/paramagnetic nanowire hetero-interfaces", Symposium on Nanotechnology, 206th Meeting of the Electrochemical Society, Honolulu, October 2004.
4. S. Pramanik and S. Bandyopadhyay, “Upstream spin transport in nanowires”, *International Conference on MEMS and Semiconductor Nanotechnology*, Indian Institute of Technology, Kharagpur, India, December 20-22, 2005.
5. S. Pramanik, C-G Stefanita and S. Bandyopadhyay, “Spin valve effect in Copper Nanowires: A Study of the Pure Elliott-Yafet Mechanism”, *International Conference on Electronic and Photonic Materials and Systems*, Kolkata, India, January 2006.
6. S. Pramanik, B. Kanchibotla and S. Bandyopadhyay, “Transverse spin relaxation times in electrochemically self assembled CdS quantum dots”, IEEE NANO 2006, Cincinnati, July 17-19, 2006.
7. S. Ramanathan, S. Bandyopadhyay, J. Nelson, J. D. Edwards, and J. Anderson, “Exciton binding energy in CdS nanowires in the presence of dielectric de-confinement”, IEEE NANO 2006, Cincinnati, July 17-19, 2006.
8. J. Wan, M. Cahay and S. Bandyopadhyay, “Effect of impurities on spin injection from a ferromagnet into a semiconductor quantum wire”, IEEE NANO 2006, Cincinnati, July 17-19, 2006.
9. S. Bandyopadhyay, S. Ramanathan, J. Moore, A. Baski, J. Edwards and J. Anderson, “Optical characterization of ZnO nanowires”, 210th Meeting of the Electrochemical Society, Cancun, Mexico, October 29 - November 3, 2006.
10. M. Cahay, K. Garre, D. J. Lockwood, J. Frazer, B. Kanchibotla, S. Pramanik, S. Bandyopadhyay, V. Semet and V. T. Binh, “Multimodal self assembly” IEEE NANO 2007, Hong Kong, July 2007.
11. J. Wan, M. Cahay and S. Bandyopadhyay, “Spin injection transistor”, IEEE NANO 2007, Hong Kong, July 2007.
12. S. Bandyopadhyay, B. Kanchibotla, S. Pramanik and M. Cahay, “Spin dephasing time in organics”, Workshop on Spins in Organics, Bologna, Italy, 8-12 September 2007.

Invited Talks and Presentations at International Conferences

1. S. Bandyopadhyay, Computing with Spin: From the Classical Era to the Quantum Era, IEEE NTC International Workshop on Quantum Device Technology, Clarkson University, Potsdam, NY, May 2004 (invited).
2. S. Bandyopadhyay, M. Cahay and S. Pramanik, Spin Transport in Quantum Wires, Engineering Conference International, Kona, Hawaii, October 19, 2004 (invited).
3. S. Bandyopadhyay, Device Applications of Spintronics, Second International Symposium on Global Network Oriented Electronics, Sendai, Japan, January 30, 2005 (invited).
4. S. Bandyopadhyay. K. Karahaliloglu and S. Pramanik, Computing with Quantum Dots and Nanowires, International Conference on Nanoscale Devices and Systems Integration, Houston, TX, April, 2005 (invited).
5. M. Cahay and S. Bandyopadhyay, Spin Injection Across Ferromagnetic/Paramagnetic Interfaces, International Conference on Nanoscale Devices and Systems Integration, Houston, TX, April, 2005 (invited).
6. S. Bandyopadhyay, Electron spin as an entity to code information, SRC-NSF Workshop, National Science Foundation, Arlington, VA, December 8, 2005 (invited).

7. S. Bandyopadhyay, Single Spin Logic, International Conference on Electronic and Photonic Materials, Devices and Systems, Calcutta University Science College, Kolkata, India, January 4, 2006 (invited).
8. S. Bandyopadhyay, Explorations in Quantum Computing, Workshop on Nanocomputation, Virginia Tech, Blacksburg, VA, May 10, 2006 (invited).
9. S. Bandyopadhyay, Self Assembled Quantum Neuromorphic Networks, Virginia Nanotech Conference (organized by University of Virginia, Virginia Tech, Old Dominion University, College of William and Mary, George Mason and Virginia Commonwealth University), Newport News, VA, June 12, 2006 (plenary).
10. S. Bandyopadhyay, Computing, Detecting, Storing and Monitoring Information with Quantum Dots, Eighth International Conference on Nanostructured Materials, Indian Institute of Science, Bangalore, India, August 2006 (invited).
11. S. Bandyopadhyay, Multifunctional Nanowires, 2006 International Electron Devices and Materials Symposia, Tainan, Taiwan, December 2006 (invited).
12. S. Pramanik, B. Kanchibotla, K. Garre, M. Cahay and S. Bandyopadhyay, Organic nano-spintronics, IEEE NANO 2007, Hong Kong, July 2007 (invited).
13. S. N. Khanna. Stable cluster motifs for nanoscale materials, International Conference on Nanoparticles, Davos, Switzerland, 2004 (invited).
14. S. N. Khanna, Potential for High Energy Nanoscale Materials Using Clusters, Second Eglin Symposium on Nanoenergetics, (organized by AFOSR and AFRL), Shalimar, Florida, March 2006.

Invited Seminars and Colloquia

1. S. Bandyopadhyay, **Spintronic Quantum Computing**, IEEE Computer Society, Richland Section, Pasco, Washington, November 11, 2004 (IEEE Distinguished Lecture).
2. S. Bandyopadhyay, **Spin Transport in Quasi One Dimensional Systems**, colloquium at Tohoku University, Sendai, Japan, Feb. 2, 2005.
3. S. Bandyopadhyay, **Counting with Spins: A Brief History of Spintronic Classical, Adiabatic and Quantum Computing**, colloquium at the Department of Physics, Virginia Commonwealth University, November 11, 2005.
4. S. Bandyopadhyay, **Spintronic Quantum Computing**, colloquium at the Department of Electronics and Telecommunication Engineering, Jadavpur University, Kolkata, India, January 9, 2006 (IEEE Distinguished Lecture).
5. S. Bandyopadhyay, **Modern spintronics**, seminar at North Carolina A&T University, Greensboro, NC, March 12, 2007.
6. S. Bandyopadhyay, **Single Spin Logic**, colloquium at the Department of Physics, University of Virginia, Charlottesville, October 18, 2007.
7. S. Bandyopadhyay, **Computing with Single Electron Spins**, colloquium at the Department of Physics, Indian Institute of Technology, Kharagpur, India, January 3, 2008.
8. S. Bandyopadhyay, **Spin based computing: classical processors**, Visionary Lecture Series, (in celebration of the platinum jubilee of the Institute) Indian Statistical Institute, Kolkata, India, January 4, 2008.

9. S. Bandyopadhyay, **Spin based computing: quantum processors**, Visionary Lecture Series, (in celebration of the platinum jubilee of the Institute) Indian Statistical Institute, Kolkata, India, January 7, 2008.
10. S. Bandyopadhyay, **Single Spin Logic**, colloquium at the Department of Physics, University of Missouri-St. Louis, March 7, 2008.
11. S. Bandyopadhyay, **Single Spin Logic**, colloquium at the Department of Electrical and Computer Engineering, Virginia Tech, March 19, 2008.
12. S. Bandyopadhyay, **Single Spin Logic,** colloquium at George Mason University, (IEEE Distinguished Lecture), April 17, 2008.

Honors and Awards

S. Bandyopadhyay was elected Fellow of the American Physical Society (APS), the Electrochemical Society (ECS) and the American Association for the Advancement of Science (AAAS) during the report period.

Citations (APS): For pioneering contributions to the device applications of nanostructures
Citation (ECS): For pioneering the application of electrochemical techniques to self assembly of nanostructures
Citation (AAAS): for distinguished contribution to the field of nanostructure device engineering

S. N. Khanna was elected Fellow of American Physical Society (APS) during the report period.

Citation: For pioneering contributions to theoretical understanding of electronic and magnetic properties of clusters as well as work on superatoms forming a new dimension to the periodic table.

S. N. Khanna also won the Distinguished Scholar Award of the College of Humanities and Sciences at Virginia Commonwealth University (2008).